OPEN

Ready for Routine

Homogeneous, High-Resolution, and Multicontrast Whole-Brain MRI at 7 Tesla in Short Scan Time With "Plug-and-Play" pTx Sequences

Jennifer Faber, MD, Daniel Paech, MD, PhD, Eberhard Pracht, PhD, Rüdiger Stirnberg, PhD, Philipp Ehses, PhD, Yannik Völzke, PhD, Daniel Löwen, MSc, Mónica Ferreira, MSc, Sascha Brunheim, MSc, Nicolas Boulant, PhD, Vincent Gras, PhD, Franck Mauconduit, PhD, Aurélien Massire, PhD, Pål Erik Goa, PhD, Laurent Lamalle, PhD, Theodor Rüber, MD, Tobias Bauer, MD, Gabor C. Petzold, MD, Julia Nordsiek, MD, Matthias Schneider, MD, Christina Schaub, MD, Thomas Klockgether, MD, Alexander Radbruch, MD, and Tony Stöcker, PhD

Background: 7T MRI received FDA/CE clearance almost 7 years ago. However, until today, it has not yet been widely adopted in clinical routine. This is mainly due to B_1 field inhomogeneities that impede whole-brain coverage. Moreover, the long scan times often associated with high-resolution imaging are an additional limiting factor.

Purpose: To combine calibration-free parallel transmit technology (pTx) using universal pulses (UP) with advanced imaging acceleration strategies to achieve homogenous multicontrast 7T MRI with whole-brain coverage and high spatial resolution in short scan time.

Materials and Methods: Ten healthy volunteers were scanned both with conventional vendor-provided sequences and with custom sequences for anatomical whole-brain imaging [T_1-weighted, T_2-weighted, FLAIR, and susceptibility-weighted]. The scan times for the 2 anatomical protocols were matched (25 minutes). In addition, a quantitative MRI protocol [multi-parametric mapping (MPM) and chemical exchange saturation transfer (CEST)] was scanned twice using custom sequences with conventional (circular polarized) and UPs, respectively, in a scan time of 2×25 minutes. Moreover, 4 patients with different neurological diseases were scanned, namely temporal lobe epilepsy, spinocerebellar ataxia, cerebral amyloid angiopathy, and glioblastoma. For the patients, only optimized custom sequences with UPs were acquired.

Results: Compared with conventional implementations, the custom sequences provide strongly improved image homogeneity and quality with significantly higher SNR and CNR across the whole brain, including cerebellum and brain stem. Moreover, UPs improve the repeatability of derived

Received for publication July 7, 2025; and accepted for publication, after revision, September 11, 2025.

From the German Center for Neurodegenerative Diseases (J.F., E.P., R.S., P.E., Y.V., D.L., M.F., S.B., G.C.P., J.N., T.K., A.R., T.S.); Department of Parkinson's Disease, Sleep and Movement Disorders, Center for Neurology (J.F.); Department of Neuroradiology, University Hospital Bonn, Bonn, Germany (J.F., D.P., Y.V., T.R., T.B., A.R.); Department of Radiology, Brigham and Women's Hospital, Harvard Medical School, Boston, MA (D.P.); University of Bonn, Bonn, Germany (M.F.); Commissariat à l'Energie Atomique, CNRS, NeuroSpin, BAOBAB, Université Paris-Saclay, Gif sur Yvette (N.B., V.G., F.M.); Diagnostic Imaging, Siemens Healthineers, Courbevoie, France (A.M.); Department of Physics, NTNU (P.E.G.); Clinic of Radiology and Nuclear Medicine, St.Olavs University Hospital, Trondheim, Norway (P.E.G.); GIGA-CRC Human Imaging, University of Liège, Liège, Belgium (L.L.); Department of Epileptology (T.R., T.B.); Department of Vascular Neurology, Center for Neurology (G.C.P., J.N.); Department of Neurosurgery (M.S.); Department of Neurooncology, Center for Neurology, University Hospital Bonn, Bonn (C.S.); Department of Neurology, University Hospital Knappschaftskrankenhaus Bochum, Ruhr University Bochum, Bochum (C.S.); Department of Physics and Astronomy, University of Bonn, Bonn, Germany (T.S.); and Center for Medical Data Usability and Translation, University Bonn, Bonn, Germany (T.R.).

J.F. and D.P. contributed equally.

Institution from which the work originated: Deutsches Zentrum für Neurodegenerative Erkrankungen (DZNE), [German Center for Neurodegenerative Diseases], Venusberg-Campus 1, 53127 Bonn, Germany.

All procedures performed in studies involving human participants were in accordance with the ethical standards of the institutional committee. Informed consent was obtained from all individual participants included in the study.

The entire UHF MRI protocol (HERTZ package) can be accessed via the Siemens C2P exchange platform for the software versions of the Siemens 7T Terra.X, Siemens 7T Terra, and the Siemens 7T Plus scanners.

Conflicts of interest and sources of funding: This work received financial support through the German Federal Ministry of Education and Research (BMBF; funding code 01ED2109A) and the Research Council of Norway (RCN, funding code 322980), both as part of the SCAIFIELD project under the aegis of the EU Joint Programme—Neurodegenerative Disease Research (JPND) and from the European Union Horizon 2020 Research and Innovation program under grant agreement 885876 (AROMA). D.P. has received funding from the Else Kroener Fresenius Foundation (2022_EKES.33). J.F. was funded within the Advanced Clinician Scientist Programme (ACCENT, funding code 01EO2107, by the German Federal Ministry of Education and Research (BMBF) and as a PI of the iBehave Network, sponsored by the Ministry of Culture and Science of the State of North Rhine-Westphalia and received funding from the National Ataxia Foundation (NAF). J.F. is a member of the European Reference Network for Rare Neurological Diseases. T.B. was funded by the Neuro-aCSis Bonn Neuroscience Clinician Scientist Program (2024-12-07). J.F. has received consultancy honoraria from Vico therapeutics and Biogen, unrelated to the present manuscript. A.M. is an employee of Siemens Healthcare SAS. D.P. is a co-founder of relios.vision GmbH, has received consultancy honoraria from Guerbet, and travel support from Siemens Healthineers, all unrelated to the present manuscript. All other authors declare that they have no conflict of interest.

Correspondence to: Jennifer Faber, MD, Deutsches Zentrum für Neurodegenerative Erkrankungen (DZNE), Venusberg-Campus 1, 53127 Bonn, Germany. E-mail: Jennifer.faber@dzne.de.

Supplemental Digital Content is available for this article. Direct URL citations are provided in the HTML and PDF versions of this article on the journal's website, www.investigativeradiology.com.

ISSN: 1536-0210/26/6106–0404
DOI: 10.1097/RLI.0000000000001252

quantitative parameters. The suggested protocol has additionally been successfully demonstrated in 4 patients with different neurological pathologies.

Conclusions: Homogeneous whole-brain 7T MRI with high spatial resolution and high image quality is possible in clinically feasible scan times. The developed protocol can be applied without any expert knowledge and is ready for clinical use. The approach could largely extend applicability of UHF MRI in neuroradiology paving the way for increased routine use of 7T MRI.

Key Words: ultra-high field, 7T, 7 Tesla, CEST, MPM, MPRAGE, pTx, infratentorial structures, neuroradiology

(*Invest Radiol* 2026;61:404–415)

Ultra-high magnetic fields (UHF) with static magnetic field strengths of $B_0 \geq 7$ Tesla (T) offer significantly higher signal-to-noise ratio (SNR) in conventional and advanced MR applications, such as iron-sensitive sequences as well as metabolic imaging. Thus, UHF MRI has an enormous potential to detect and monitor structural and biochemical alterations of the brain at an unprecedented level of detail that cannot be achieved with 3T.[1–4] However, these clear advantages are opposed by technical shortcomings that have hampered a widespread application of UHF MRI to date. Major limitations are transmit field (B_1) inhomogeneities at UHF which fundamentally degrade image quality, particularly at the excentric infratentorial brain regions of the field-of-view (FOV), to such an extent that the diagnostic image quality in those brain regions limits broader clinical use of UHF MRI until today.[5,6] The B_1 inhomogeneities result from radiofrequency (RF) interferences and dielectric resonances observed at high proton Larmor frequency (300 MHz at 7T). Image artifacts induced by B_1 inhomogeneity can be mitigated by the parallel transmission (pTx) technology, where the total B_1 field is generated by several independent transmit channels. It provides the required degrees of freedom to generate spatially homogenous excitation (flip angle), as needed for most MRI techniques. However, the B_1 field variations are subject-specific, which needs to be taken into account for the application-specific pTx RF pulse design. This may require the acquisition of calibration scans (B_0 and B_1 field mapping per channel), and numerical pulse optimization, before the actual examination can start, which results in prolonged scan times. Although fast B_0 and B_1 mapping exists nowadays,[7,8] acquisition and pulse-calculation still require on the order of a minute or more. More importantly, online pulse calculation is prone to failure due to factors such as motion during the calibration scans or unsuccessful pulse optimization, for example, resulting from segmentation or masking failure, or from numerical simplification introduced to speed up convergence. To overcome such problems, several calibration-free approaches have been suggested, which enable high-quality UHF MRI without the need of calibration procedures. In this context, so-called universal pulses (UPs)[9] have been proposed, where a database of B_0 and B_1-maps from several subjects is used for subject-independent pTx RF pulse optimization. For this study we acquired a large calibration database and successfully designed tailored UPs for all custom sequences, forming a comprehensive protocol for anatomical neuroimaging (T_1w, T_2w, FLAIR, SWI) of the entire brain including brainstem and cerebellum in consistently high resolution and quality, complemented by a set of quantitative and metabolic imaging approaches (QSM, MPM, CEST). In addition, the in-house developed MRI sequences have enhanced acceleration capabilities. This is beneficial for high-resolution imaging at 7T, where conventional spatial encoding either requires long scan times or diminishes image quality. Compared with scan-time-matched acquisitions with the vendor-product sequences on the Siemens Terra or 7T Plus systems, the image quality has been improved with significantly better SNR and CNR for all considered supra- and infratentorial regions. Comparisons with product implementations on the new Terra.X system have not yet been carried out, as such a system was not available to the authors. This aspect is addressed at the end of the Discussion section.

MATERIALS AND METHODS

Sequence Design

RF Pulse Design for B_1 Homogenization

A calibration database of high-quality field maps was acquired for subsequent UP design using the vendor-provided double-echo 3D-GRE sequence for B_0-mapping and our custom 3D-DREAM for B_1 mapping.[7] The protocol details are provided in the supporting information. Currently, calibration data from 82 healthy subjects acquired at 3 different 7T sites (Bonn, Trondheim, Liège) are included in the database. The presented results are based on UPs derived from a subset of 30 subjects, which is sufficiently large to ensure robustness against variations but yet small enough to maintain manageable computational demands. We chose an equal number of subjects from each site by sorting them based on their reference voltage, which is the most influential factor affecting pulse performance, and evenly distributed 10 subjects from each site across this range.

The UP design is based on the GRAPE algorithm,[10] which provides short RF pulses, effectively mitigating B_1 inhomogeneities over the whole brain while minimizing sensitivity to off-resonance effects. Specifically, UPs were computed for (water-selective) excitation and inversion,[11] spin-echo refocusing,[12] and non-adiabatic inversion for T_2-FLAIR imaging.[13] Several pTx methods have been proposed to mitigate the B_1 inhomogeneity for CEST saturation.[14–16] In this work, magnetization saturation for CEST and MPM was realized with the recently published PUSHUP approach[17] – a calibration-free extension of the PUSH method[18] – where saturation homogenization is achieved through multiple sub-pulses with individually optimized B_1-shims. All UPs were designed by incorporating Specific Absorption Rate (SAR) limits and, in some cases, sequence acquisition parameters into account as constraints for the GRAPE optimization. The UPs can still be applied in case of SAR-affecting protocol changes (eg, reduced TR), which may require downscaling of flip angles. In such situations, better results are usually obtained by redesigning the UPs with different constraints. Accordingly, just like product sequences typically provide the user a selection of different circular polarized (CP) mode pulses, our sequences provide different UP designs for different target flip angle ranges or SAR constraints.

Anatomical and Quantitative Sequences

Three custom sequences were implemented for anatomical imaging: MPRAGE for T_1-weighted contrast,[19] SPACE for T_2-weighted and FLAIR contrast,[20] as well as 3D echo-planar imaging (EPI) for susceptibility-weighted imaging (SWI) which also provides quantitative susceptibility maps (QSM).[21] Beyond that, the quantitative MRI protocol consists of custom sequences for MPM and CEST, both using our fast 3D-EPI readout.[22,23] MPM acquires 3 multi-echo gradient-echo images with different weightings—proton density (PDw), longitudinal relaxation time (T_1w), and magnetization transfer (MTw)—followed by quantitative analysis to provide parametric maps of T_1, T_2^*, PD and MT_{sat}.[24] CEST is a molecular imaging technique that detects exchangeable protons on low concentration solute molecules through the water signal by RF labeling of these protons and subsequent transfer to water protons.[25] Targeting at sub-millimeter isotropic resolution, all custom sequences use 3D k-space encoding with

TABLE 1. Imaging Protocol and Corresponding Sequence Parameters

	TA [min]	TR [ms]	TE [ms]	FOV [mm³]	resolution [mm]	acceleration	pTx-mode flip angle	sequence specific
anatomical								
MPRAGE vendor	5:50	3000	1.9	230x230x172	0.6	GRAPPA 4x1	CP 4 °	- TI=1.1s
MPRAGE custom	5:46	3000	2.4	230x230x172	0.6	CAIPI 2x2 $_{z1}$ ES, CS	UP 4 °	- TI=1.1s
SPACE vendor	4.08	4000	369	230x230x172	0.6	CAIPI 3x2 $_{z1}$ ES	CP vFA	- vendor vFA
SPACE custom	4:28	4000	369	230x230x172	0.6	CAIPI 2x2 $_{z1}$ ES, CS	UP vFA	- EPG vFA
FLAIR vendor	6:08	6000	369	230x230x172	0.6	CAIPI 3x2 $_{z1}$ ES	CP vFA	- TI=2s - vendor vFA
FLAIR custom	6:40	6000	369	230x230x172	0.6	CAIPI 2x2 $_{z1}$ ES, CS	UP vFA	- TI=2s - EPG vFA
SWI vendor	5:40	31	19	166x202x22	0.4	GRAPPA 3x1	CP 13 °	- 3D-GRE
SWI custom	5:38	40	19	204x204x166	0.4	CAIPI 2x2 $_{z1}$ EF=17	UP 13 °	- 3D-EPI - QSM
quantitative (custom)								
MPM							UP (& CP)	- 3D-EPI
PDw	4:01	33.5	4.6,11.6,	216x216x172	0.6	CAIPI 1x3 $_{z1}$	4 °	- PUSHUP
T1w	4:01	33.5	18.6,25.6			EF=4,PF=80%	25 °	(-QSM)
MTw	5:39	47.5					6 °	
CEST	7:37	4700	6.7	216x206x180	1.6	CAIPI 4x2 $_{z1}$ EF=24,PF=75%	UP (& CP) 10 °	- 3D-EPI - 44xΔf - 2xB_1 - PUSHUP

The upper part shows acquisition parameters for the custom and vendor anatomical sequences of the anatomical protocol. The lower part shows the sequence parameters of the quantitative protocol consisting of the MPM and CEST acquisitions, which both take advantage of fast 3D-EPI readout and PUSHUP for homogenous saturation. Resolution denotes the isotropic voxel size for all sequences.

CP indicates circular polarized; CS, compressed sensing; EF, EPI factor; ES, elliptical sampling; FOV, field-of-view; TA, acquisition time; TE, echo time; TI, inversion time; TR, repetition time; UP, universal pulses; vFA, variable flip angle.

combinations of different acceleration techniques: (i) 2D-CAIPIRINHA parallel imaging along both phase encoding axes, (ii) partial Fourier, (iii) elliptical sampling, (iv) Echo Planar Imaging (EPI), and (v) compressed sensing (CS).[26] Further details about the sequence implementation, calibration database, UP design, and image post-processing are given in the supporting information.

MR Examination

MR Protocol

On the basis of the custom MRI sequences, a comprehensive neuro-MRI protocol with high spatial resolution and short scan time was implemented on a Siemens 7T scanner (Siemens Healthineers, MAGNETOM 7TPlus) equipped with an 8Tx/32Rx head coil (Nova Medical, Wilmington, MA). MPRAGE, SPACE, FLAIR, and SWI form the anatomical protocol. Table 1 (top part) shows the protocol parameters for these contrasts in comparison to a protocol based on vendor sequences, which were approximately time-matched to our optimized custom sequences. (Exact matching was not possible due to limited flexibility of the vendor sequences' view ordering and acceleration capabilities). The vendor sequences only serve as a reference for comparison, such a protocol would not be utilized in practice. For instance, standard MPRAGE in CP mode is rarely used at 7T. Instead, the MP2RAGE sequence is commonly used as it corrects B_1 inhomogeneity by signal division utilizing a second readout.[27] Naturally, this comes at the expense of a prolonged acquisition time. As approximate time-matching was our goal for the reference protocol, MP2RAGE was not considered. Inspecting Table 1 in detail, the largest difference between our custom protocol and the vendor-based reference can be observed for SWI, where our custom sequence is based on the advanced 3D-EPI approach, whereas the vendor sequence uses a conventional gradient-echo (3D-GRE or FLASH) sequence. As the latter has no EPI-factor for acceleration, a time-matched protocol with the same coverage is not possible. Thus, we strongly reduced the head-to-feet FOV of the vendor sequence for the time-matched acquisition, resulting in a 22mm slab. The lower part of Table 1 shows the quantitative protocol, that is, the sequence parameters for CEST and MPM. Note that the CEST sequence is repeated with two B_1 scales for both acquisitions, CP and UP, to correct for saturation homogenization. Although this is required for accurate quantification with CP-mode transmission, PUSHUP-CEST provides good quantification results already with a single scaling, which would half the acquisition time.[17] To have a fair comparison, two B_1 scales were used for both acquisitions. The image reconstruction is performed online on the MR system for all sequences. Here, a dedicated reconstruction workflow is used in case of compressed sensing acquisitions (MPRAGE and SPACE), otherwise the vendor-provided image reconstruction pipelines are used (cf. supporting information for more details).

Subject Selection and Examinations

The entire MRI protocol (anatomical and quantitative) was scanned on 10 healthy volunteers (mean age 28±3.5 years). The anatomical protocol was acquired with our custom sequences

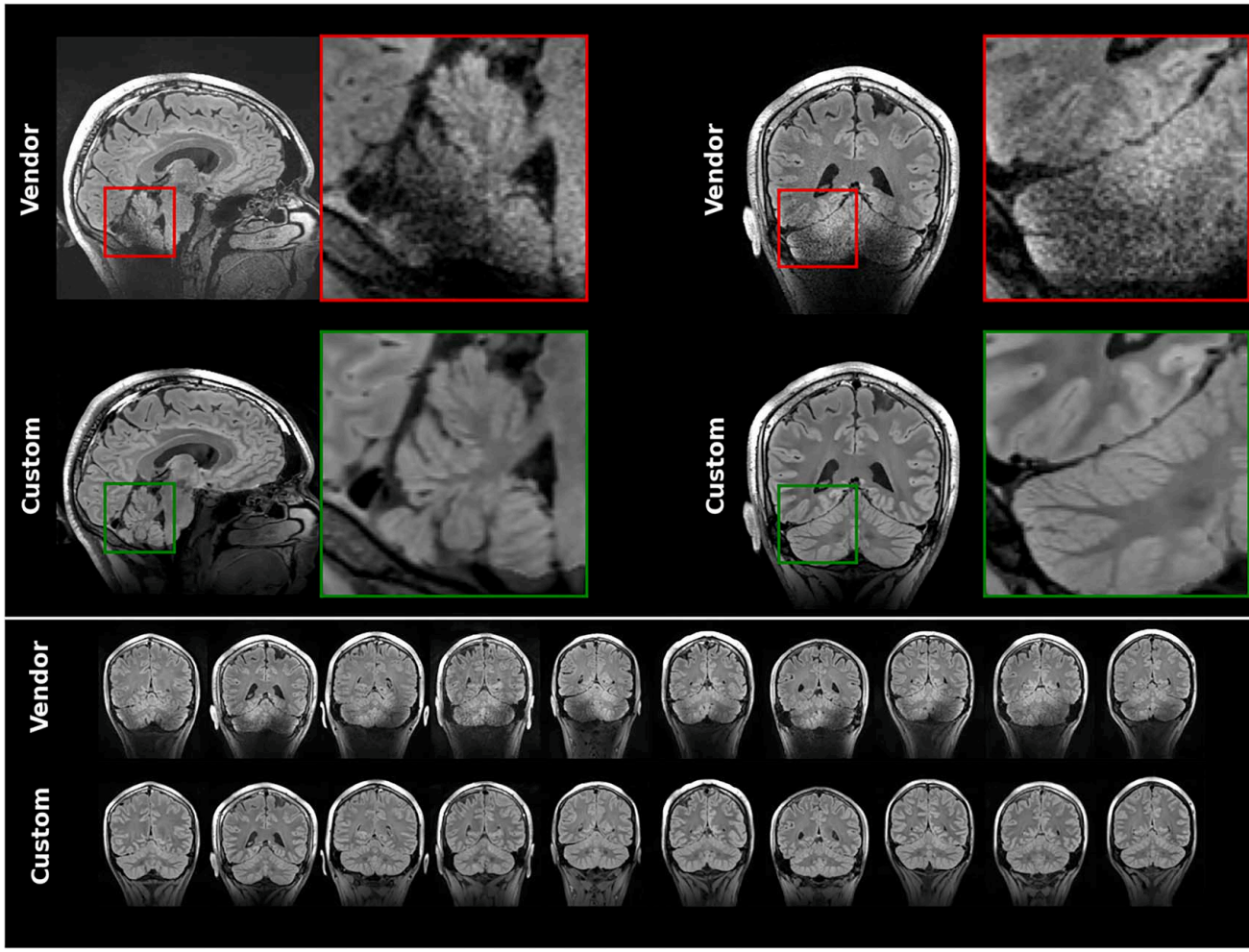

FIGURE 1. Intraindividual comparison of FLAIR images obtained with the vendor and custom sequences. The close-up views in the top panel highlight the superior image homogeneity and quality of the custom FLAIR. In the bottom panel, the coronal views of pairwise intraindividual comparisons demonstrate that image quality impairments due to CP-mode acquisition occurred consistently with the vendor sequence, whereas image quality and homogeneity could be improved reliably with the custom sequence in all healthy subjects.

and with the time-matched vendor sequences. The custom quantitative sequences, CEST and MPM, were scanned with UP pTx and conventional CP mode on all healthy volunteers. In addition, a test-retest repeatability study was performed for the quantitative protocol on 3 healthy volunteers. Here, the CEST and MPM sequences with CP-mode and UP transmission were scanned twice with a short break and repositioning of the subject in between. To estimate the precision of the quantitative parameters, the voxel-wise coefficient of variation (COV) between test and retest scans was calculated. More details are given in the supporting information.

Four exemplary neurological patients were studied with a protocol limited to the optimized custom version to keep the burden on patients low. Patient 1 was a 30-year-old female with temporal lobe epilepsy due to left hippocampal sclerosis. Patient 2 was a 67-year-old male patient with a genetically confirmed spinocerebellar ataxia type 3 (SCA3). Patient 3 was a 62-year-old male with a probable cerebral amyloid angiopathy according to the Boston criteria 2.0.[28] Patient 4 was a 59-year-old female patient with a newly diagnosed glioblastoma. All subjects gave their informed consent following local institutional review board regulations in accordance with the Declaration of Helsinki.

RESULTS

Healthy Controls

Figure 1 shows representative intraindividual T_2 FLAIR images obtained with the custom and vendor sequence, respectively. The close-up views demonstrate the superior image homogeneity in the cerebellum as well as the improved contrast and image quality for the custom sequence. Homogeneity and contrast improvements mainly result from the UPs, whereas reduced parallel-imaging artifacts and reduced noise can be attributed to the improved acceleration and reconstruction techniques. Together this leads to improved overall image quality. The lower part of Figure 1 shows that these improvements were observed consistently across all subjects. Figure 2 provides an overview of all contrasts from the anatomical imaging protocol for one healthy volunteer, again intraindividually comparing images from the respective custom and vendor

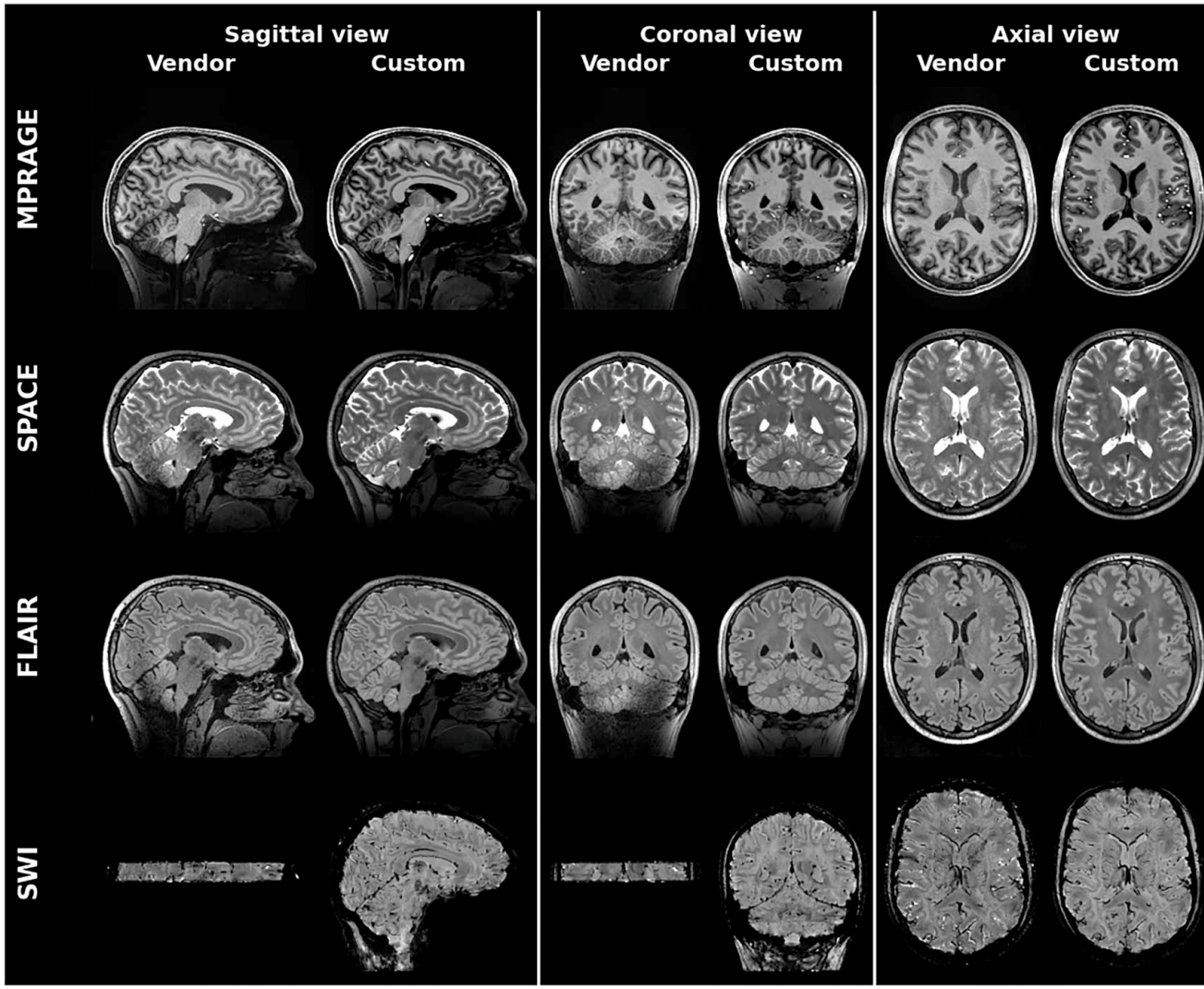

FIGURE 2. Anatomical images of one healthy volunteer. The columns compare sagittal, coronal, and axial views of acquisitions with vendor and custom sequences, respectively. The rows show contrasts obtained with different sequences: T_1-weighting with MPRAGE, T_2-weighting with SPACE, fluid-suppressed T_2-weighting with FLAIR, and SWI with 3D-GRE (vendor) and 3D-EPI (custom). The vendor SWI can only cover a small FOV in the same acquisition time as compared with the custom SWI (cf. Methods section).

sequences. Image inhomogeneity in infratentorial regions is apparent for all vendor sequences due to conventional CP-mode transmission. Figure 3 depicts QSM and SWI post-processing results acquired with the custom 3D-EPI sequence. Here, the high spatial isotropic resolution of 0.4 mm allows to visualize fine anatomical details. Table 2 shows ROI group analysis results for the anatomical imaging protocol. The SNR of the custom MPRAGE sequence is strongly improved in comparison to the vendor implementation, which results from the enhanced image acceleration capabilities of the custom sequence. The SNR improvement of custom sequences is also present for all other contrasts, although to a lesser extent. Moreover, all WM/GM contrast metrics were improved in all sequence comparisons (except for SWI, which does not target WM/GM contrast).

Figures 4, 5 show representative results from the quantitative imaging protocol for the custom CEST and MPM sequences. Both figures compare UP versus CP-mode transmission, where especially the CEST maps underline the importance of pTx for whole-brain homogenization. Overall, excellent quality can be observed for all quantitative MRI maps obtained with UPs. Results of the statistical group analysis are provided in the supplementary material (Table S1, Supplemental Digital Content 1, http://links.lww.com/RLI/B82). Figure 6 shows representative results from the test-retest study with the quantitative imaging protocol. As can be seen from the plot, low COVs on the order of 10% and, therefore, reasonable repeatability is observed for most parameters. Only the COV of MPM-MT_{sat} is substantially larger, which means that this parameter is difficult to estimate at 7T, as previously reported in a CP-mode study.[23] Other high-resolution 7T studies tend to omit MPM-MT_{sat} estimation but yield similar COVs for the other MPM parameters.[29] Most important for this study is the improvement (ie, lower COVs) obtained with UP instead of CP transmission, which can be especially observed in the cerebellum for several contrasts (cf. Fig. 6). A detailed region-of-interest group analysis is provided in the supplementary material (Table S2,

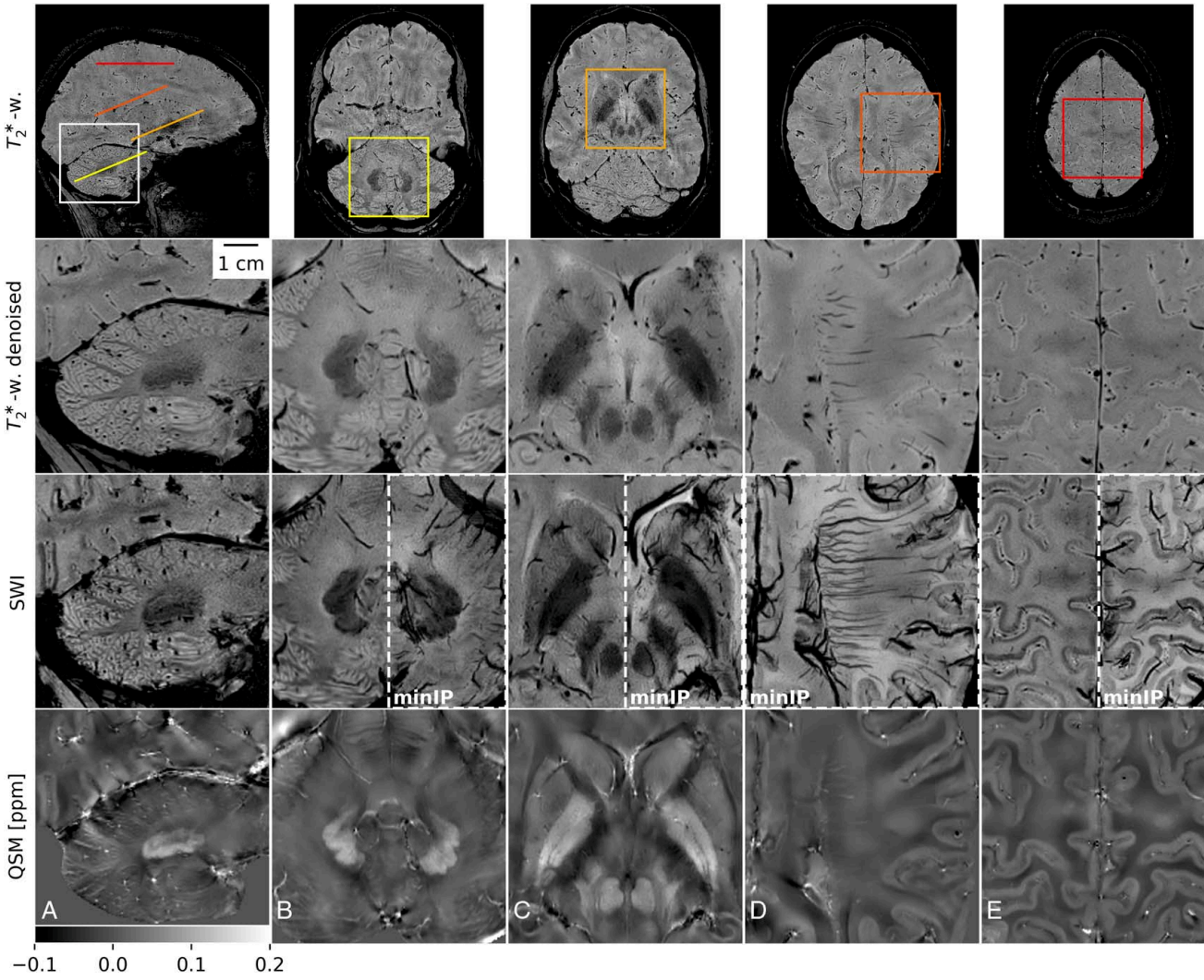

FIGURE 3. SWI and QSM images of one healthy volunteer, reconstructed from the custom 3D-EPI acquisition at 0.4 mm isotropic resolution. A–E, show views at different heights and reslicing angles as indicated in the whole-brain sagittal view (top left). Rows 2–4 show magnified views as indicated in the top row. From top to bottom: T_2^*-weighted magnitudes of preprocessed data (row 1), after complex-valued denoising (row 2), corresponding SWIs and 5.6 mm minimum intensity projections (minIP) in selected views (row 3), and quantitative susceptibility maps (row 4). From left to right, the dentate nucleus, red nuclei, substantia nigra, striatum incl. pallidum, medullary veins and the motor cortex with cortical veins are displayed at high resolution and contrast in the different maps.

Supplemental Digital Content 1, http://links.lww.com/RLI/B82), which shows that UP transmission results in lower COVs than CP transmission for most of the quantitative parameters and especially in infratentorial brain regions.

Patient Examples

The four patient cases underline the feasibility of the protocol and demonstrate high whole-brain image quality (cf. Fig. 7) in various neurological diseases, namely hippocampal sclerosis in epilepsy, degeneration of deep cerebellar nuclei and infratentorial atrophy in hereditary ataxia, microbleeds in cerebral amyloid angiopathy, and left-sided temporal glioblastoma.

DISCUSSION

The availability of UHF MRI is steadily increasing, and it has been CE/FDA approved for neuro and musculoskeletal (MSK) diagnostics (fall 2017). The advantages of UHF MRI with improved SNR and CNR for imaging of anatomical details in high resolution are evident. Moreover, metabolic imaging approaches benefit in particular from the higher field strength and increased spectral resolution, as shown by numerous applications in neurological diseases.[5,30]

However, at the same time, the high field strength is associated with technical limitations that impede homogenous image quality across the entire brain. Accordingly, its widespread use in clinical routine is still limited. In this study, we demonstrated that fast high-resolution whole-brain neuro-MRI is feasible at 7T. The presented UHF neuroimaging protocol is based on custom MRI sequences that utilize pTx excitation with "plug-and-play" universal pulses (UPs) and advanced spatial encoding acceleration, enabling high-quality and artifact-free whole-brain imaging in short scan time. The comprehensive one-hour protocol consists of 4 structural scans (T_1-w, T_2-w, FLAIR, SWI) and 2 quantitative scans (MPM and CEST) providing tissue parameter maps and metabolic information. Compared

TABLE 2. Group Mean Values of Region-Specific Image Quality Metrics Obtained From 10 Healthy Subjects

Metric	MPRAGE Vendor (SD)	MPRAGE Custom (SD)	SPACE Vendor (SD)	SPACE Custom (SD)	FLAIR Vendor (SD)	FLAIR Custom (SD)	SWI Vendor (SD)	SWI Custom (SD)
GM SNR	8.93 (0.42)	24.68 (4.11)	65.03 (22.51)	91.64 (25.37)	48.65 (17.75)	73.92 (22.73)	15.76 (1.77)	35.66 (1.89)
WM SNR	14.26 (0.81)	42.14 (6.97)	50.4 (17.85)	64.72 (18.58)	41.01 (15.3)	58.96 (18.69)	13.17 (1.93)	31.63 (2.4)
CB SNR	4.35 (0.34)	28.74 (4.72)	55.27 (20.56)	85.15 (23.95)	38.52 (14.49)	69.81 (22.01)	10.19 (4.48)	30.45 (3.79)
BS SNR	10.39 (1.36)	39.6 (6.04)	54.92 (19.07)	66.82 (18.6)	41.44 (14.81)	60.55 (18.99)	10.01 (3.07)	26.62 (2.59)
dGM SNR	13.35 (1.16)	32.98 (5.66)	56.73 (20.01)	72.58 (20.29)	43.31 (16.05)	62.93 (19.36)	10.88 (1.85)	25.8 (2.48)
total SNR	9.29 (0.64)	29.87 (4.81)	55.47 (20.3)	76.27 (22.08)	39.12 (14.19)	61.15 (19.15)	11.65 (2.07)	28.57 (2.18)
WM/GM CNR	4.25 (0.38)	13.93 (2.32)	11.68 (3.93)	21.47 (5.87)	6.1 (2.17)	11.93 (3.74)	3.57 (1.2)	2.37 (0.33)
WM/GM MC*100	21.59 (1.24)	24.38 (0.68)	11.79 (0.91)	16.15 (1.2)	6.18 (1.03)	9.33 (1.27)	9.0 (2.69)	4.89 (2.58)
WM/GM CJV*100	127.19 (9.07)	88.84 (4.08)	185.27 (16.99)	160.89 (15.47)	298.07 (52.98)	182.58 (24.87)	524.56 (163.02)	794.77 (543.9)

Overall, small SDs compared with mean values reflect a high reproducibility across subjects. Note that WM/GM metrics (last 3 rows) are of limited value for SWI sequences (last 2 columns), which do not target a WM/GM contrast. All region-specific estimates for the custom SWI were restricted to the FOV of the vendor SWI to allow a fair comparison (cf. Fig. 2).

BS indicates brainstem; CB, cerebellum; CJV, coefficient of joint variation; CNR, contrast-to-noise ratio; dGM, deep gray matter nuclei; GM, gray matter; MC, Michelson contrast; SNR, signal-to-noise ratio; WM, white matter.

with conventional approaches at 7T all contrasts demonstrated significantly improved SNR and CNR in all regions considered. In addition, UPs improve the precision of derived quantitative parameter maps, as shown in test-rest experiments.

In all patient cases, UPs lead to homogeneous tissue contrast and parameter quantification throughout the brain, also for the case of a large tumor (cf. Fig. 7D). We are currently collecting more data to investigate the UP performance in patients. So far, we have not observed a single case with remaining B_1-induced image inhomgeneities. We attribute this to two important properties of our UP design: first, a large database of high-quality calibration data with diverse anatomy is used, and second, UPs are designed with the largest possible number of degrees of freedom (DoF) using the GRAPE algorithm.[10] With respect to the first property, it seems that the B_1 variability due to different anatomies in the database is sufficient to cope with the B_1 variability caused by lesions—this observation is not surprising considering the smooth, person-specific variations in B_1, which are typically little affected by pathology. On the basis of our experience, the second property is, however, even more important: "general UPs" such as GRAPE fully exploit the pTx dynamics by arbitrary simultaneous gradient and channel-wise RF waveforms. This results in short, optimized pulses that are less sensitive to off-resonances, for example, compared with kT-points or SPINS pulses.[31,32] The computation of these pulses takes several hours or up to several days in case of a large database, even when utlizing fast multiprocessing computers. As UPs are precomputed, the calculation time is not relevant for clinical applications, where UPs lead to fast, robust and calibration-free B_1-homogenization. In addition to these promising properties of UPs, there have also been remarkable recent advances in subject-specific pulse design. The FOCUS approach originally proposed online-customized pulses for the MPRAGE sequence, which are initialized by kT-points UPs.[33] FOCUS pulses are quickly calculated online utilizing fast patient-specific B_1 and B_0 calibrations scans, resulting in better performance than the initial UPs. However, so far it has not been investigated if rapid online-calculated pulses can also improve more sophisticated general UPs such as GRAPE. More recently, FOCUS pulses were proposed for T_2-weighted imaging with the SPACE sequence,[34] where the pulse design also fully exploits the maximum available DoF, similar to GRAPE. Another study showed that the approach leads to strongly improved image homogeneity in patients when compared with CP-mode acquisition.[35] Again, a comparison to advanced GRAPE-UPs has not yet been carried out and should be investigated in the future. In addition, it would be very interesting to use the UPs proposed in this work for SPACE-FOCUS initialization, to find out if rapid online customization can still improve highly optimized calibration-free pulses. Obviously, online-customized approaches have the advantage that subject-specific information is considered. However, there is little time available to acquire the information with sufficient quality and then make use of it during online pulse design. Moreover, the same property may turn into a disadvantage, if, for example, motion or insufficient B_0-shimming degrades the calibration data. In conclusion, online-customized pulses are promising, and it remains to be determined whether they can already robustly outperform UPs for neuroradiologic applications. Once 7T will reach out to imaging the body, subject-specific pulse design may become unavoidable. For neuroimaging applications, calibration-free UPs provide a robust and easy-to-use alternative, as demonstrated in this work.

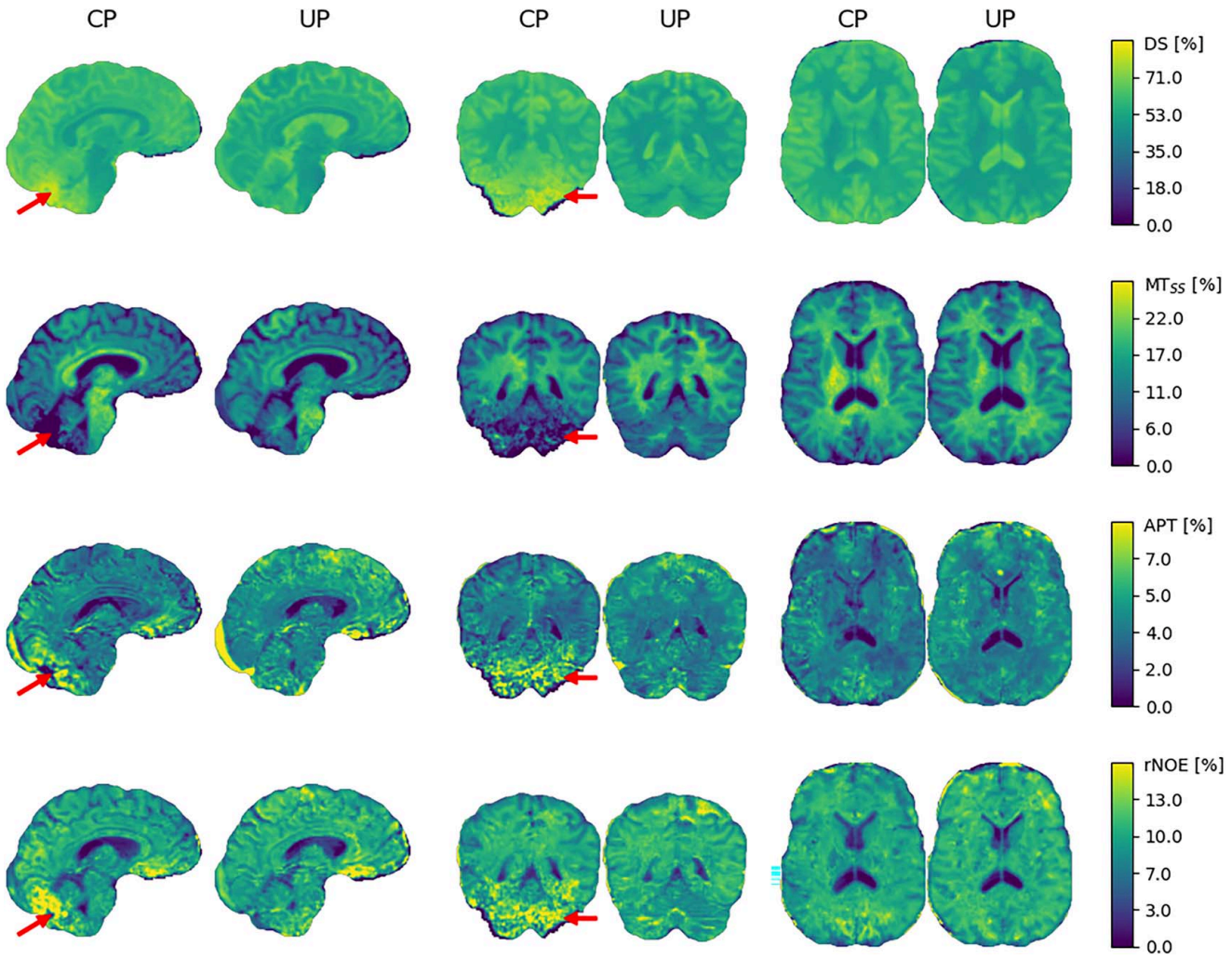

FIGURE 4. Quantitative CEST results of one healthy volunteer. Each quantitative parameter (percentage peak amplitude) is given in one row, from top to bottom: direct saturation (DS), semi-solid Magnetization Transfer (MT_{SS}), Amide Proton Transfer (APT), relayed Nuclear-Overhauser-Enhanced (rNOE). The columns compare sagittal, coronal, and axial views of acquisitions using conventional circular polarized (CP) mode and universal pulses (UP) for excitation and saturation, respectively. The saturation with CP-mode transmission fails in the cerebellum resulting in artifacts for all contrasts (cf. red arrows).

Next to pTx homogenization, high-resolution acquisitions with short scan times are a key feature of the proposed protocol. The structural scans achieve 0.6 mm isotropic resolution (SWI: 0.4 mm) in 4 to 7 minutes each. As previously shown, long scan times at 7T using only conventional parallel-imaging techniques, or T_1-weighted structural imaging with MP2RAGE (eg, TA = 9:32 minutes for 0.75 mm isotropic resolution), can lead to increased motion artifacts compared with typical 3T imaging, potentially limiting clinical value.[36] Particularly strong motion artifacts were not observed with the sequences proposed in this study, which may be related to acquisition times comparable to typical 3T protocols at 1 mm isotropic resolution.

The sequences can be combined in a modular manner. They are suitable for a wide range of clinical and scientific applications in neurology and neurodegeneration. The use of UHF MRI has been recognized, for example, in epilepsy, especially for the detection of epileptogenic lesions.[3,37] In addition, 7T MRI has very high sensitivity for detecting subtle hemorrhagic and vascular changes, which are essential in the diagnostic workup of patients with cerebral amyloid angiopathy (CAA).[38] Recently, this has become of particular interest in the context of patients with Alzheimer's undergoing amyloid-targeting therapies, where amyloid-related imaging abnormalities (ARIA-H), like microbleeds and superficial siderosis, are a concern.[39] However, for a diagnostic workup imaging of the entire brain in high resolution without local artifacts is a prerequisite. Today, additional 3T MRI scans are often still acquired to assess the typical blind spots of 7T MRI, which this work aims to overcome. Neurodegenerative diseases where the neuropathology is emphasized in, but not restricted to, the infratentorial structures are sporadic and hereditary ataxias. Imaging of the cerebellum and brainstem has so far been most affected by the technical shortcomings of UHF MRI with pronounced signal loss in these regions. At the same time, anatomical structures such as the tiny folia of the cerebellar cortex and the serrated shape of the dentate nucleus benefit enormously from higher resolution and iron-sensitive imaging. In

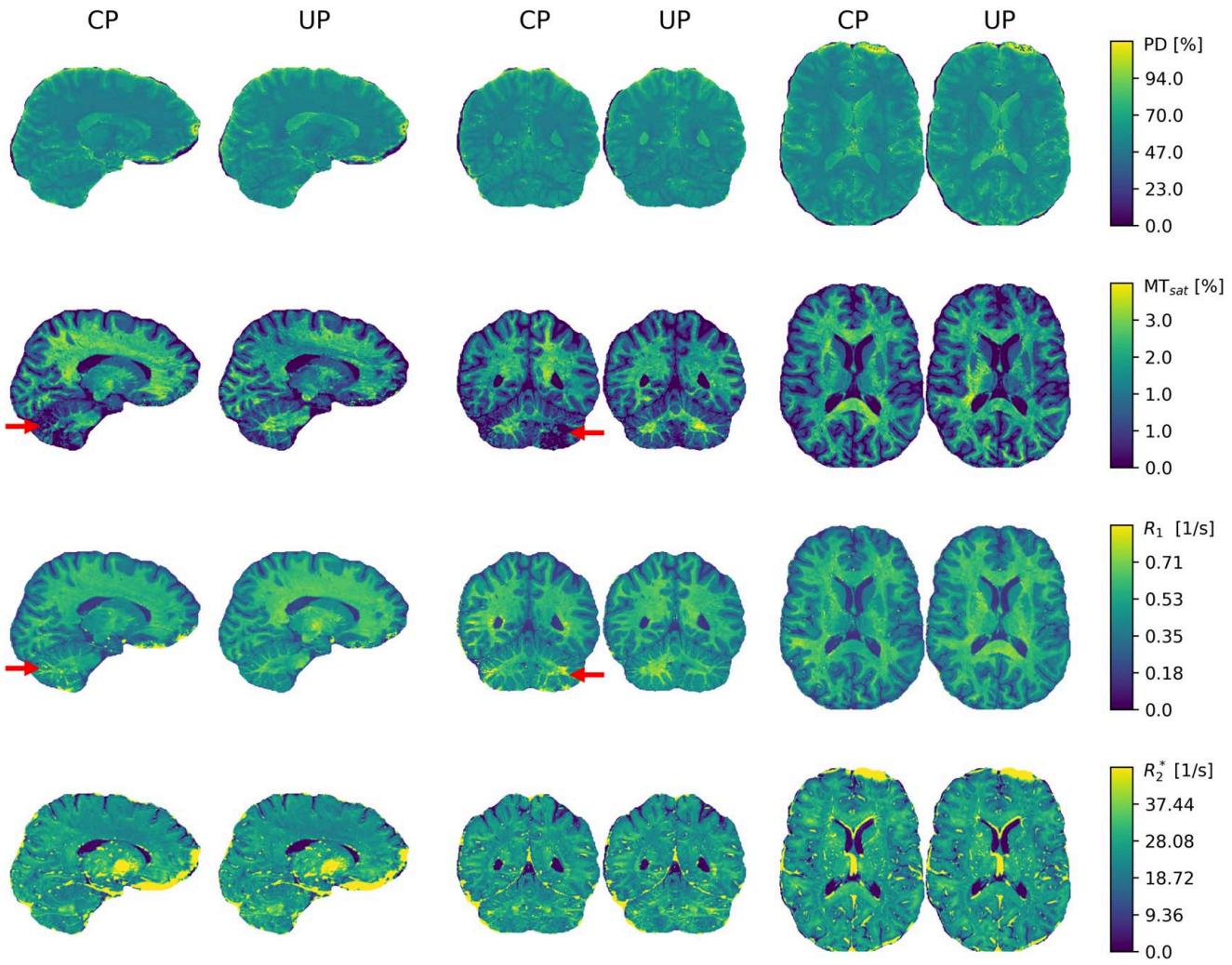

FIGURE 5. Quantitative MPM results of one healthy volunteer. Each quantitative parameter is given in one row, from top to bottom: Proton Density (PD), Magnetization Transfer Saturation (MT_{sat}), longitudinal relaxation rate (R_1), and effective transverse relaxation rate ($R_2{}^*$). For MPM, the advantage of pTx is less pronounced, and both transmission modes, CP and UP, provide similar results. Largest differences can be observed for MT_{sat} and R_1, where CP-mode saturation and excitation were not sufficient in all areas of the cerebellum (cf. red arrows).

the light of upcoming gene therapies for the most common autosomal-dominantly inherited ataxias,[40] there is an urgent need for imaging biomarkers that can capture subtle, early changes. In addition to these examples, UHF offers tremendous opportunity to significantly improve structural and metabolic neuroimaging due to improved SNR and CNR, thus advancing the imaging of pathological changes. Given the diagnostic approval and increasing availability of UHF scanners the presented comprehensive protocol offers an enormous potential to pave the way to a broad use of UHF MRI in clinical routine and research in neurology.

By design, UPs are specific to the RF coil. Therefore, the entire protocol presented in this study is limited to the usage with the 8-channel Tx/32-channel Rx Nova coil, which is the vendor-provided pTx head coil. For a different coil, the UPs must be redesigned from scratch, which requires the acquisition of a new calibration database from ~20 to 30 subjects. For example, high-quality B_1 and B_0 maps can be rapidly acquired (TA < 1 min) using the 3D-DREAM sequence.[7] As UP calculation needs to be performed only once for the new database, we do consider this a manageable limitation. However, UP design requires experience and knowledge, so this step cannot easily be performed by 7T users unfamiliar with pTx pulse design. Interested sites are encouraged to contact the corresponding author of this paper, as we are eager to extend our approach to different hardware configurations.

Our custom sequences and protocols are available for the Siemens 7T Plus, the 7T Terra, and the 7T Terra.X scanners. However, comparisons between our protocol and vendor-provided product sequences were only performed on the 7T Plus system (which is technically equivalent to the Terra). The Terra.X system now provides a pTx-enabled MPRAGE product sequence based on online-customized FOCUS pulses, which would allow such a comparison in the future. All other custom sequences presented in this study do not yet have a pTx vendor-product counterpart. This is likely to change in the near future

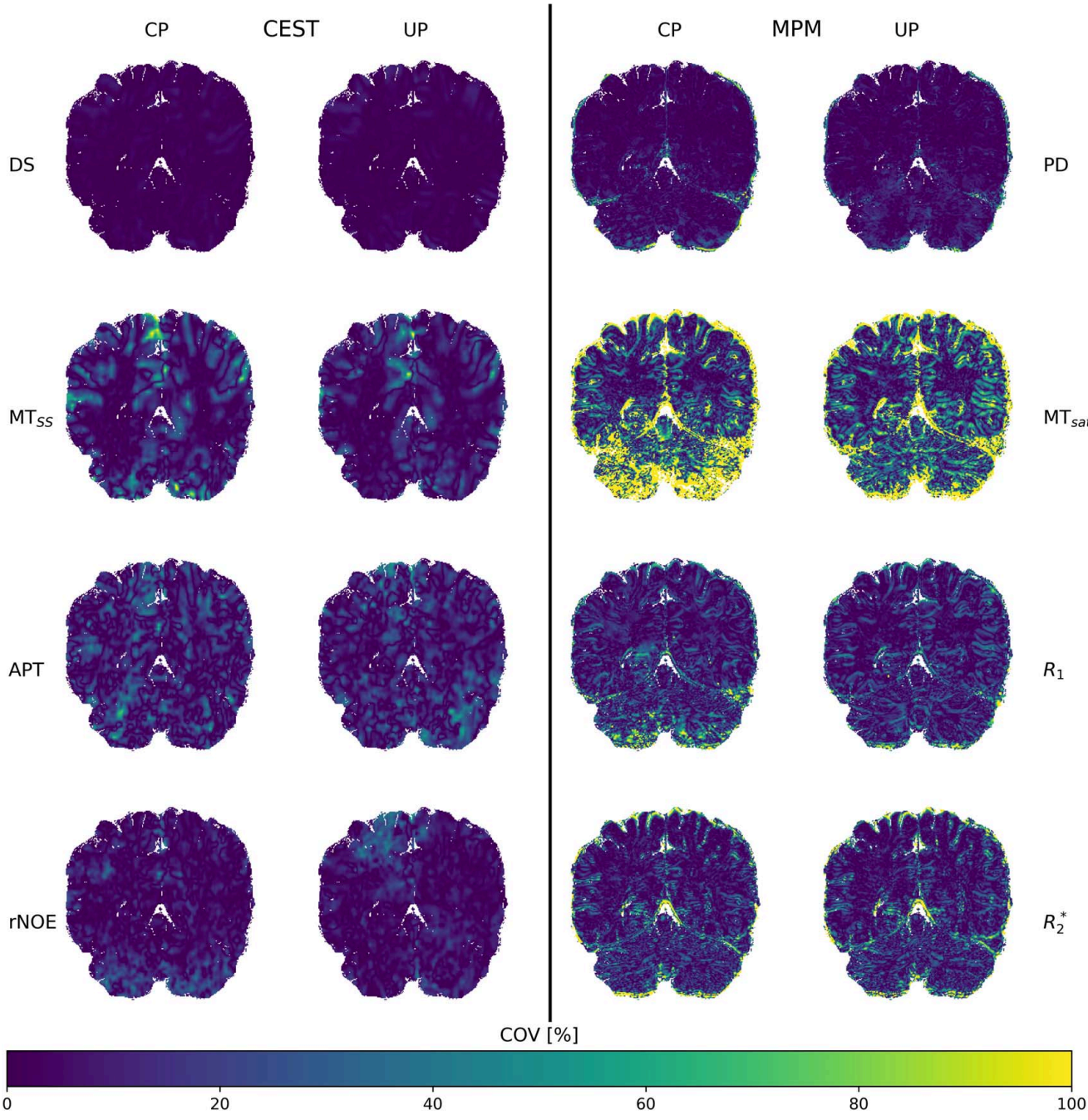

FIGURE 6. Results of the test-retest repeatability study for one healthy volunteer. The plot shows the coefficient of variation (COV) of all quantitative CEST and MPM parameters for both transmission modes, CP and UP. For most contrasts COVs < 10% and therefore a good repeatability is observed. Only MPM-MT_{sat} shows substantially larger values. Overall, the CP and UP results are similar, but UP provide notably smaller COVs in the cerebellum.

for the SPACE sequence, again potentially implementing the FOCUS approach. Once available, corresponding comparisons with our sequences will be conducted in collaboration with Terra.X sites. In addition, it should be noted that only the Terra.X system has FDA/CE clearance for pTx product sequences. Nevertheless, usage of our custom sequences remains restricted to (clinical) research applications on all systems.

Another important research question for the future is the extension of our sequence package to deep-learning (DL) based image reconstruction, which enables very high acceleration factors for anatomical brain imaging.[41,42] Such promising developments are complementary to the here-proposed parallel-imaging and compressed sensing methods. Thus, DL can be implemented on top, potentially providing even higher total acceleration. In the

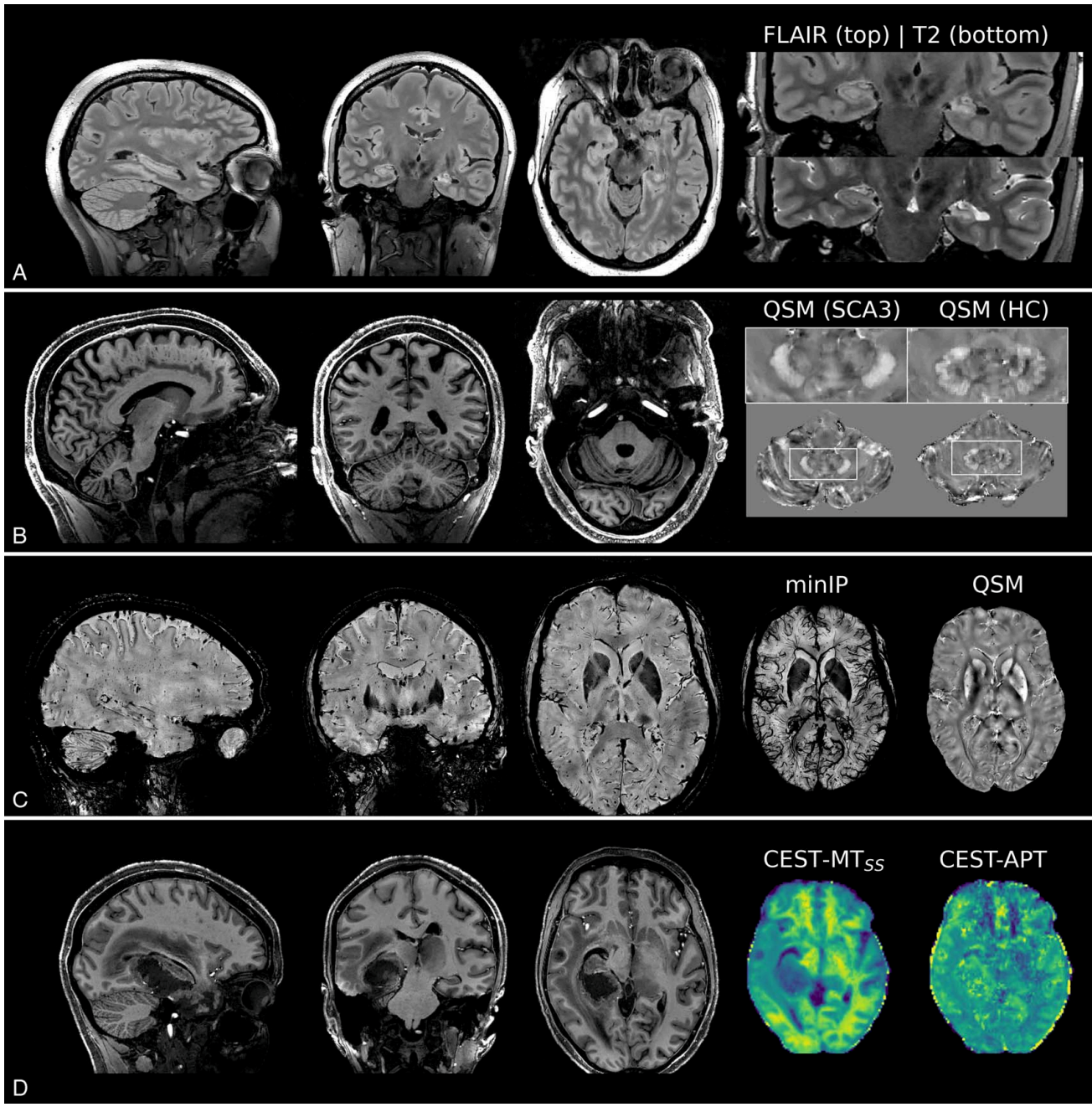

FIGURE 7. Patient example data obtained with the proposed custom protocol. A, Hippocampal sclerosis in an epilepsy patient (patient 1). B, Cerebellar atrophy and degeneration of the dentate nucleus in patient 2, suffering from the most common autosomal-dominantly inherited ataxia, spinocerebellar ataxia type 3 (SCA3). The right plot compares QSM of the SCA3 patient and a healthy control (HC). C, Patient 3 shows cortical microbleeds typical for cerebral amyloid angiopathy (CAA). D, Patient 4 that was scanned one day before neurosurgical resection of the left hemispheric temporal glioblastoma (WHO Grade 4, IDH wildtype, MGMT promotor hypermethylation) demonstrating excellent image quality of the custom sequences, also in this case of altered brain structure. In addition, CEST contrasts provide molecular information on amide proton transfer (APT) and semi-solid magnetization transfer (MT_{SS}).

future, we are planning to apply DL to our custom sequence package and compare open DL-based image reconstruction tools[43] with the vendor-provided DL reconstruction, as for example, available on the 7T Terra.X system. In addition, DL-based reconstruction needs careful validation in the case of quantitative imaging, as intended with the here-proposed protocol.

REFERENCES

1. Obusez EC, Lowe M, Oh S-H, et al. 7T MR of intracranial pathology: preliminary observations and comparisons to 3T and 1.5T. *NeuroImage*. 2018;168:459–476.
2. Trattnig S, Springer E, Bogner W, et al. Key clinical benefits of neuroimaging at 7 T. *Neuroimage*. 2018;168:477–489.

3. Van Lanen RHGJ, Colon AJ, Wiggins CJ, et al. Ultra-high field magnetic resonance imaging in human epilepsy: a systematic review. *NeuroImage Clin*. 2021;30:102602.
4. Wang I, Oh S, Blümcke I, et al. Value of 7T MRI and post-processing in patients with nonlesional 3T MRI undergoing epilepsy presurgical evaluation. *Epilepsia*. 2020;61:2509–2520.
5. Platt T, Ladd ME, Paech D. 7 Tesla and beyond: advanced methods and clinical applications in magnetic resonance imaging. *Invest Radiol*. 2021; 56:705–725.
6. Regnery S, Knowles BR, Paech D, et al. High-resolution FLAIR MRI at 7 Tesla for treatment planning in glioblastoma patients. *Radiother Oncol*. 2019;130:180–184.
7. Ehses P, Brenner D, Stirnberg R, et al. Whole-brain B1-mapping using three-dimensional DREAM. *Magn Reson Med*. 2019;82:924–934.
8. Kent JL, Dragonu I, Valkovič L, et al. Rapid 3D absolute B_1^+ mapping using a sandwiched train presaturated TurboFLASH sequence at 7 T for the brain and heart . *Magn Reson Med*. 2023;89:964–976.
9. Gras V, Vignaud A, Amadon A, et al. Universal pulses: a new concept for calibration-free parallel transmission. *Magn Reson Med*. 2017;77: 635–643.
10. Van Damme L, Mauconduit F, Chambrion T, et al. Universal nonselective excitation and refocusing pulses with improved robustness to off-resonance for Magnetic Resonance Imaging at 7 Tesla with parallel transmission. *Magn Reson Med*. 2021;85:678–693.
11. Löwen D, Pracht ED, Stirnberg R, et al. Interleaved binomial k_T -points for water-selective imaging at 7T . *Magn Reson Med*. 2022;88:2564–2572.
12. Gras V, Mauconduit F, Vignaud A, et al. Design of universal parallel-transmit refocusing k_T -point pulses and application to 3D T_2 -weighted imaging at 7T . *Magn Reson Med*. 2018;80:53–65.
13. Gras V, Pracht ED, Mauconduit F, et al. Robust nonadiabatic T2 preparation using universal parallel-transmit kT-point pulses for 3D FLAIR imaging at 7 T. *Magn Reson Med*. 2019;81:3202–3208.
14. Tse DHY, Da Silva NA, Poser BA, et al. Inhomogeneity mitigation in CEST using parallel transmission. *Magn Reson Med*. 2017;78:2216–2225.
15. Liebert A, Zaiss M, Gumbrecht R, et al. Multiple interleaved mode saturation (MIMOSA) for B_1^+ inhomogeneity mitigation in chemical exchange saturation transfer . *Magn Reson Med*. 2019;82:693–705.
16. Liebert A, Tkotz K, Herrler J, et al. Whole-brain quantitative CEST MRI at 7T using parallel transmission methods and correction. *Magn Reson Med*. 2021;86:346–362.
17. Völzke Y, Akbey S, Löwen D, et al. Calibration-free whole-brain CEST imaging at 7T with parallel transmit pulse design for saturation homogeneity utilizing universal pulses (PUSHUP). *Magn Reson Med*. 2025;93:630–642.
18. Leitão D, Tomi-Tricot R, Bridgen P, et al. Parallel transmit pulse design for saturation homogeneity (PUSH) for magnetization transfer imaging at 7T. *Magn Reson Med*. 2022;88:180–194.
19. Brenner D, Stirnberg R, Pracht ED, et al. Two-dimensional accelerated MP-RAGE imaging with flexible linear reordering. *Magma*. 2014;27:455–462.
20. Pracht ED, Feiweier T, Ehses P, et al. SAR and scan-time optimized 3D whole-brain double inversion recovery imaging at 7T. *Magn Reson Med*. 2018;79:2620–2628.
21. Stirnberg R, Deistung A, Reichenbach JR, et al. Rapid submillimeter QSM and R2* mapping using interleaved multishot 3D-EPI at 7 and 3 Tesla. *Magn Reson Med*. 2024;92:2294–2311.
22. Akbey S, Ehses P, Stirnberg R, et al. Whole-brain snapshot CEST imaging at 7 T using 3D-EPI. *Magn Reson Med*. 2019;82:1741–1752.
23. Wang D, Ehses P, Stöcker T, et al. Reproducibility of rapid multi-parameter mapping at 3T and 7T with highly segmented and accelerated 3D-EPI. *Magn Reson Med*. 2022;88:2217–2232.
24. Tabelow K, Balteau E, Ashburner J, et al. hMRI—a toolbox for quantitative MRI in neuroscience and clinical research. *Neuroimage*. 2019;194:191–210.
25. Zhou J, Payen J-F, Wilson DA, et al. Using the amide proton signals of intracellular proteins and peptides to detect pH effects in MRI. *Nat Med*. 2003;9:1085–1090.
26. Stöcker T. Recommendations for neuro MRI acquisition strategies. *Adv Magn Reson Technol Appl*. 2021;4(Elsevier):3–20.
27. Marques JP, Kober T, Krueger G, et al. MP2RAGE, a self bias-field corrected sequence for improved segmentation and T1-mapping at high field. *Neuroimage*. 2010;49:1271–1281.
28. Charidimou A, Boulouis G, Frosch MP, et al. The Boston criteria version 2.0 for cerebral amyloid angiopathy: A multicentre, retrospective, MRI–neuropathology diagnostic accuracy study. *Lancet Neurol*. 2022;21:714–725.
29. Vaculčiaková L, Podranski K, Edwards LJ, et al. Combining navigator and optical prospective motion correction for High-quality 500 μm resolution quantitative Multi-parameter mapping at 7T. *Magn Reson Med*. 2022;88:787–801.
30. Kraff O, Fischer A, Nagel AM, et al. MRI at 7 tesla and above: demonstrated and potential capabilities. *J Magn Reson Imaging*. 2014;33: 13–33.
31. Cloos M A, Boulant N, Luong M, et al. K(T) -points: Short three-dimensional tailored RF pulses for flip-angle homogenization over an extended volume. *Magn Reson Med*. 2011:67:72–80.
32. Malik SJ, Keihaninejad S, Hammers A, et al. Tailored excitation in 3D with spiral nonselective (SPINS) RF pulses. *Magn Reson Med*. 2012;67: 1303–1315.
33. Herrler J, Liebig P, Gumbrecht R, et al. Fast online-customized (FOCUS) parallel transmission pulses: a combination of universal pulses and individual optimization. *Magn Reson Med*. 2021;85: 3140–3153.
34. Piredda GF, Sleight E, Yu T, et al. Individually optimized dynamic parallel transmit pulses for 3D high-resolution SPACE imaging at 7T. *Magn Reson Med*. 2025;94:1616–1625.
35. Middlebrooks EH, Herrler J, Piredda GF, et al. Clinical Implementation of Dynamic Parallel Transmission in 7T Brain MRI: Improved Homogeneity and Contrast Using SPACE Sequences. *Am J Neuroradiol*. 2025;46:2438–2445.
36. Wang ZI, Oh S-H, Lowe M, et al. Radiological and clinical value of 7T MRI for evaluating 3T-visible lesions in pharmacoresistant focal epilepsies. *Front Neurol*. 2021;12:591586.
37. Opheim G, Van Der Kolk A, Bloch KM, et al. 7T epilepsy task force consensus recommendations on the use of 7T MRI in clinical practice. *Neurology*. 2021;96:327–341.
38. Ni J, Auriel E, Martinez-Ramirez S, et al. Cortical localization of microbleeds in cerebral amyloid angiopathy: an ultra high-field 7T MRI study. *J Alzheimer Dis*. 2014;43:1325–1330.
39. Koemans EA, Van Etten ES, Van Opstal AM, et al. Innovative magnetic resonance imaging markers of hereditary cerebral amyloid angiopathy at 7 Tesla. *Stroke*. 2018;49:1518–1520.
40. Faber J, Berger M, Wilke C, et al. Stage-dependent biomarker changes in spinocerebellar ataxia type 3. *Ann Neurol*. 2023;95:400–406.
41. Liu Z, Zhou X, Tao S, et al. Application of deep learning accelerated image reconstruction in T2-weighted turbo spin-echo imaging of the brain at 7T. *AJNR Am J Neuroradiol*. 2025;46:1517–1520.
42. Liu Z, Patel V, Zhou X, et al. Deep-learning reconstruction for 7T MP2RAGE and SPACE MRI: improving image quality at high acceleration factors. *AJNR Am J Neuroradiol*. 2025;46:2446–2454.
43. Blumenthal M, Luo G, Schilling M, et al. Deep, deep learning with BART. *Magn Reson Med*. 2023;89:678–693.

